Electronic Supplementary Material

Fe-doped $SrTiO_3$ perovskites: exploring their applications in photocatalytic dye degradation and supercapacitors

Prabodh Ch Paul[1], Dev Kumar Mahato (✉)[1],
and Mrityunjoy Mahato (✉)[2]

1 Department of Physics, National Institute of Technology Patna, Patna 800005, Bihar, India
2 Physics Division, Department of Basic Sciences and Social Sciences, School of Technology, North-Eastern Hill University, Shillong 793022, Meghalaya, India

E-mails: devk@nitp.ac.in (D.K.M.), mmahato@nehu.ac.in (M.M.)

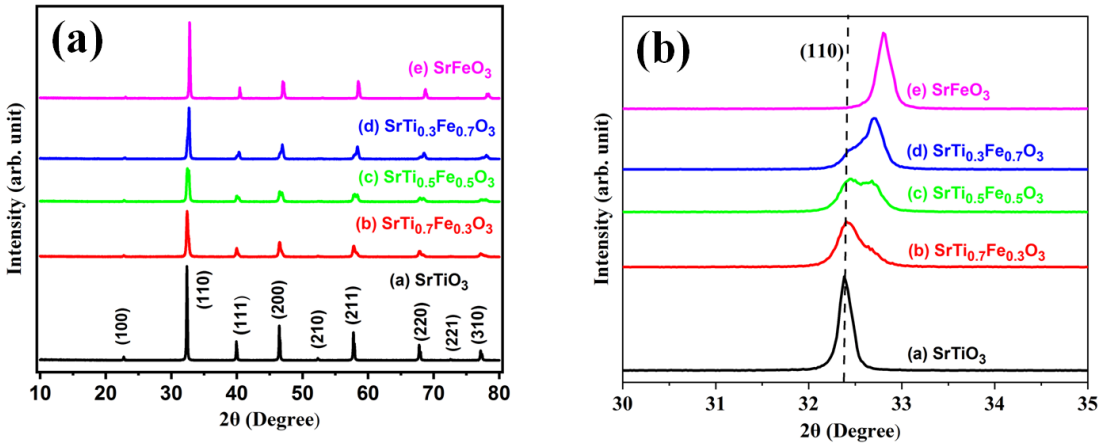

Fig. S1 (a) XRD patterns and **(b)** 2θ positions of the (110) plane for STO, SFO, and Fe-doped STO.

Table S1 XRD peak positions for pure STO, SFO, and Fe-doped STO samples (STFO1, STFO2, STFO3, SFO)

(*hkl*)	2θ				
	Pure STO	STFO1	STFO2	STFO3	SFO
(100)	22.76°	22.77°	22.80°	22.92°	23.02°
(110)	32.40°	32.40°	32.50°	32.70°	32.80°
(111)	39.96°	39.98°	40.05°	40.31°	40.44°
(200)	46.48°	46.51°	46.71°	46.91°	47.05°
(210)	52.79°	–	–	–	53.09°
(211)	57.79°	57.84°	58.12°	58.37°	58.52°
(220)	67.83°	67.88°	68.22°	68.58°	68.74°
(221)	72.58°	–	–	–	–
(310)	77.20°	77.17°	77.66°	78.08°	78.22°

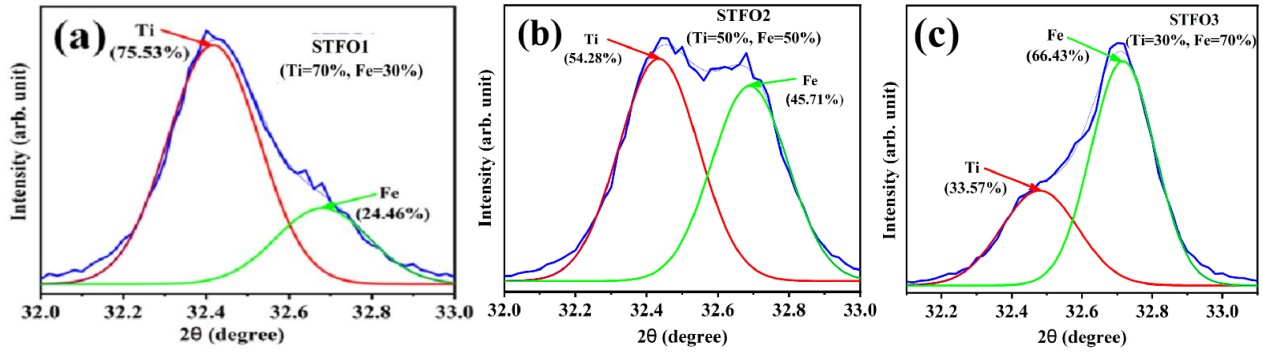

Fig. S2 XRD patterns of the (110) plane for **(a)** STFO1, **(b)** STFO2, and **(c)** STFO3 with deconvoluted peaks determining molar proportions of Ti and Fe.

The molar proportions of Ti and Fe determined from XRD and EDS are compared with those from the raw materials, which are summarized in Table S2. The molar ratios of Ti to Fe obtained from XRD are close to theoretical ones (70:30, 50:50, and 30:70 for STFO1, STFO2, and STFO3, respectively). However, the molar ratios determined from EDS show some discrepancies, which may be due to the non-homogeneous doping status of Fe into STO and the fact that EDS is not a very much quantitative technique but a mostly qualitative technique for elemental analysis.

Table S2 Comparative molar proportions of elements from raw materials, XRD, and EDS

Sample	Determination from raw materials		Determination from XRD		Determination from EDS	
	η(Ti)/%	η(Fe)/%	η(Ti)/%	η(Fe)/%	η(Ti)/%	η(Fe)/%
STFO1	70	30	75.53	24.47	42.18	57.42
STFO2	50	50	54.28	45.71	80.72	19.28
STFO3	30	70	33.57	66.43	7.52	92.48

Note: η is the molar proportion.

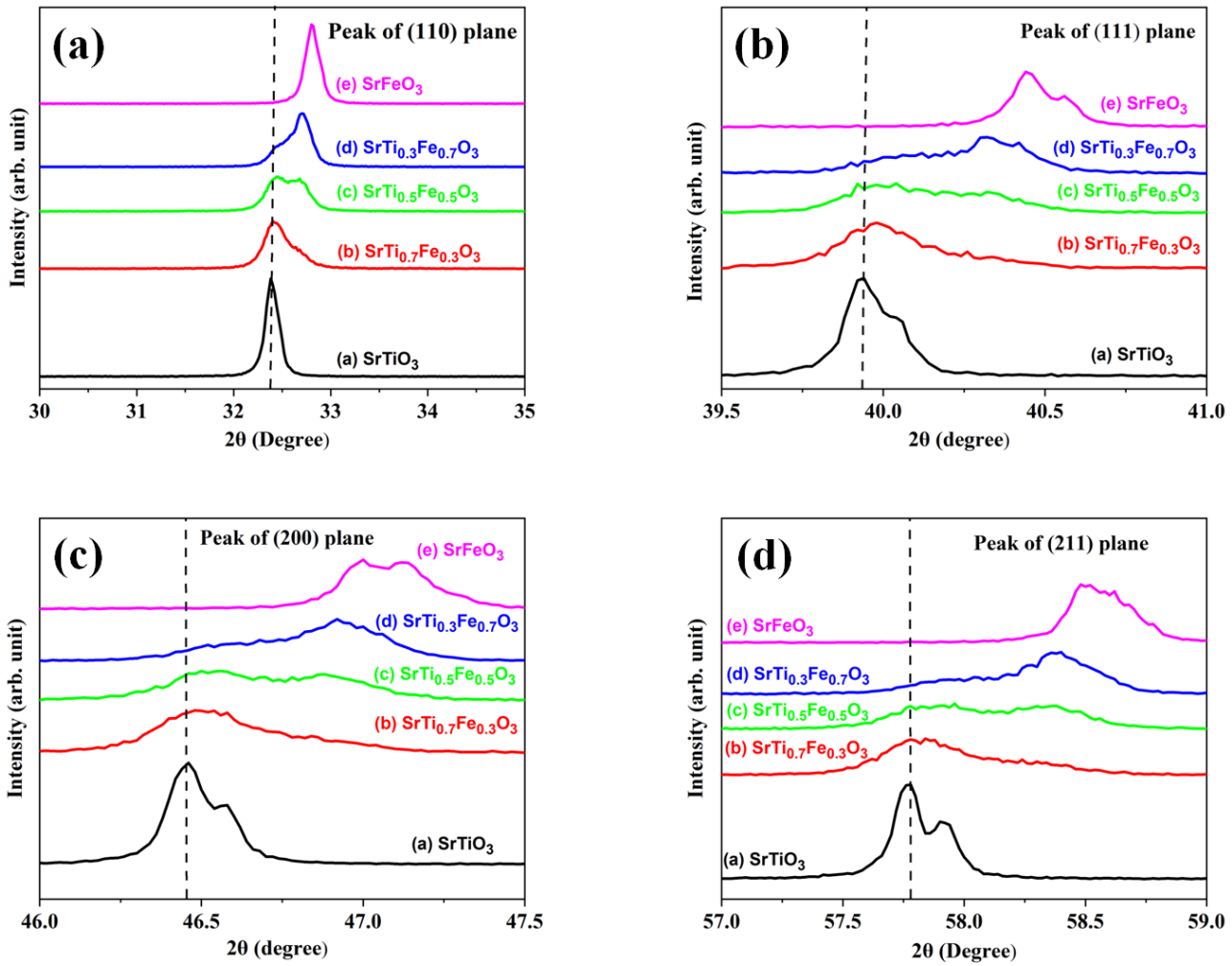

Fig. S3 XRD peak shifting of **(a)** (110), **(b)** (111), **(c)** (200), and **(d)** (211) planes for STO, STFO1, STFO2, STFO3, and SFO, probably due to the doping of Fe into STO [S1].

Table S3 Reliability factors of full prof fitting for SFO and Fe-doped STO

Sample [a)]	Reliability factors				
	R_p	R_{wp}	R_e	χ^2	$a = b = c$
STFO1	22.6	29.0	17.1	2.86	3.9022
STFO2	22.1	28.6	17.6	2.63	3.8899
STFO3	25.2	30.3	17.6	2.97	3.8750
SFO	14.4	22.1	18.8	1.39	3.8659

a) All samples belong to the Pm3m group.

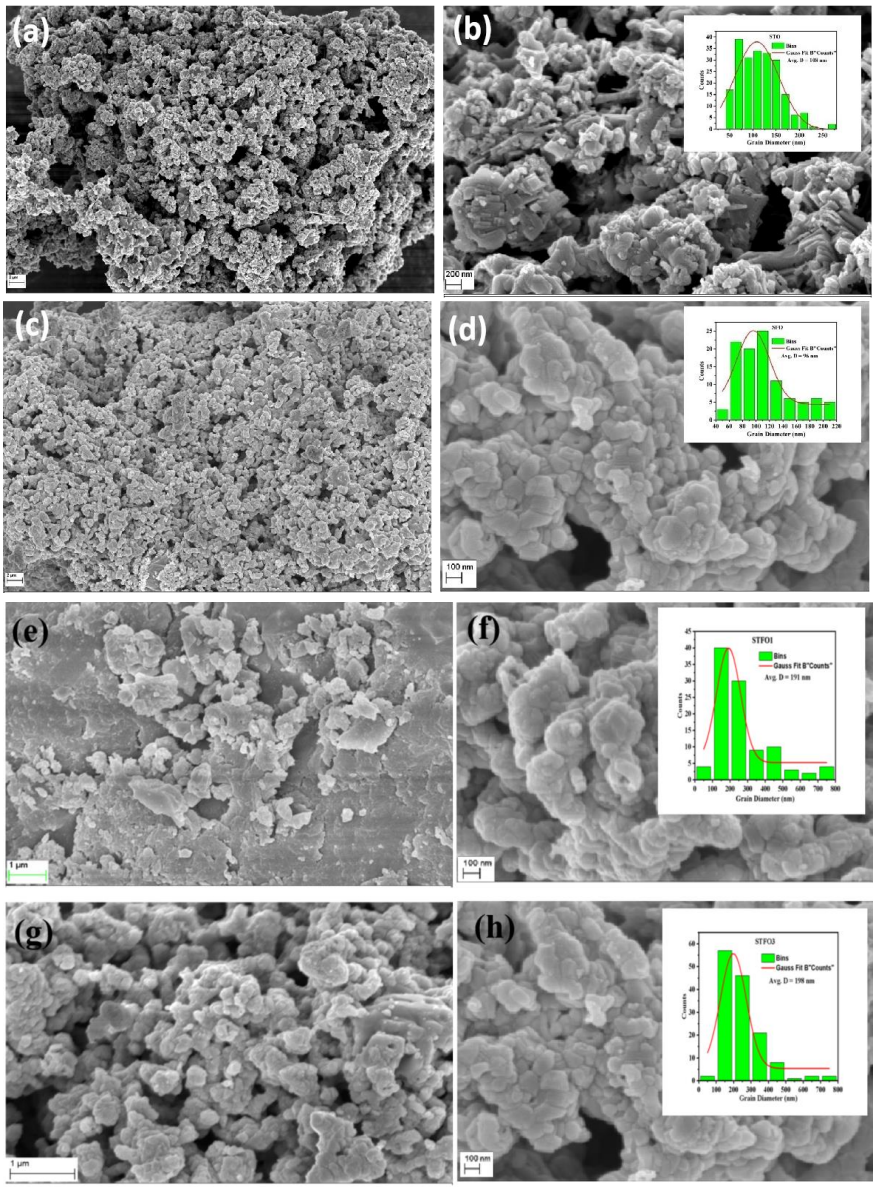

Fig. S4 Low-resolution (left panels) and high-resolution (right panels) SEM images for **(a)(b)** STO, **(c)(d)** SFO, **(e)(f)** STFO1, and **(g)(h)** STFO3, with insets showing their average particle sizes of 108, 96, 191, and 198 nm, respectively, besides corresponding distributions of grain sizes [S2].

The Sr 3d XPS spectrum for either STFO2 or STFO3 was deconvoluted into two Gaussian lines, with the Sr 3d-doublet lines at binding energies of 130.81 and 133.81 eV for STFO2 while 131.91 and 133.15 eV for STFO3, corresponding to Sr $3d_{5/2}$ and Sr $3d_{3/2}$, respectively (Figs. S5(a) and S5(e)) [S3]. It is observed from Fig. S5(b) and S5(f) that the fitted peaks located at 459.05 and 464.79 eV for STFO2 while 456.98 and 463.00 eV for STFO3 correspond to Ti $2p_{3/2}$ and Ti $2p_{1/2}$, respectively [S4]. Fe 2p XPS spectra characterized with doublet peaks for STFO2 and STFO3 are shown in Figs. S5(c) and S5(g), respectively, among which doublet peaks of Fe $2p_{3/2}$ and Fe $2p_{1/2}$ are located at 712.55 and 726.37 eV for STFO2, while at 710.33 and 723.84 eV for STFO3, respectively [S5]. Each O 1s XPS spectrum yields two deconvoluted peaks corresponding to different binding energy positions, as depicted in Fig. S5. Stronger peaks in both Figs. S5(d) and S5(h) are associated with oxygen ions at 530.74 and 531.43 eV for STFO2 and STFO3, respectively, which are related to oxygen in the perovskite structure of Fe-doped STO, indicating that such oxygen ions remain coordinated in the TiO_6 octahedra. Weaker peaks, at 533.46 and 528.34 eV for STFO2 and STFO3, respectively, are due to an intermediate oxidation state for oxygen and may be related to carbonate compounds as well as defects such as oxygen vacancies and chemical adsorption [S6].

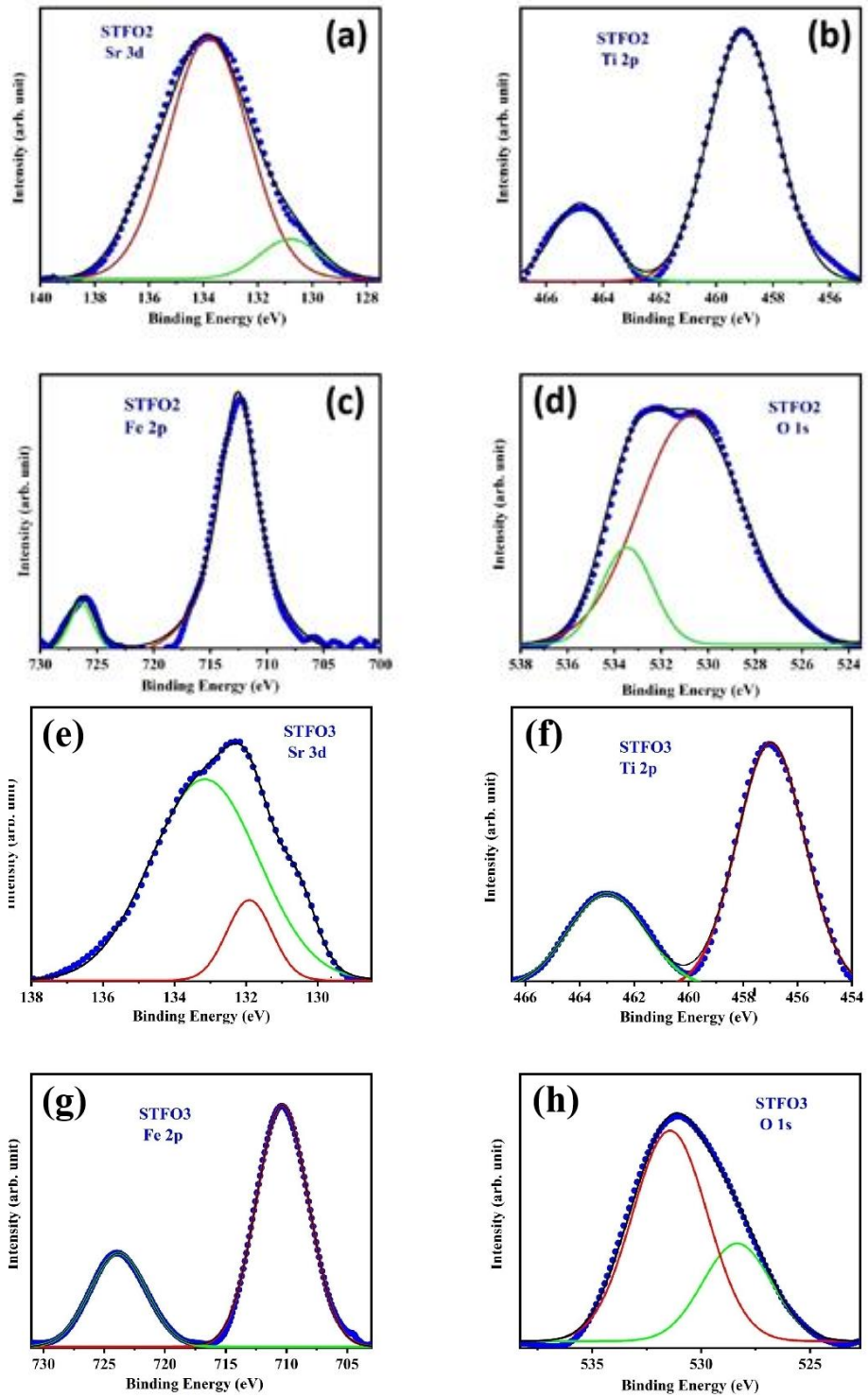

Fig. S5 (a)(e) Sr 3d, **(b)(f)** Ti 2p, **(c)(g)** Fe 2p, and **(d)(h)** O 1s core-level XPS spectra for STFO2 and STFO3 samples.

Table S4 Comparative XPS data for Fe-doped STO photocatalysts

Sample	Peak position/eV								Ref.
	Sr $3d_{5/2}$	Sr $3d_{3/2}$	Ti $2p_{3/2}$	Ti $2p_{1/2}$	Fe $2p_{3/2}$	Fe $2p_{1/2}$	O 1s	O 1s	
Fe-doped STO	132.8	–	458.4	–	710.3	720.3	–	–	[S3]
Fe-doped STO	132.7	134.4	458.1	464.0	710.2	723.5	529.6	531.3	[S4]
Fe co-doped STO	133.0	–	458.6	–	710.05	723.5	529.5	531.4	[S5]
Fe-doped STO	–	–	–	–	710.9	724.4	–	–	[S7]
STFO1	133.71	135.12	459.72	465.60	712.88	721.66	531.94	532.64	This work
STFO2	130.81	133.81	459.05	464.79	712.55	726.37	530.74	533.46	
STFO3	131.91	133.15	456.98	463.00	710.33	723.84	528.34	531.43	

Figure S6 shows the shifting of Sr, Ti, Fe, and O XPS peaks for pure STO and Fe-doped STO samples possibly due to the change of the doping concentration, which was also proven by Li et al. who observed that peaks of Sr and Ti were slightly shifted to lower binding energies due to the increased concentration of doped Fe [S8].

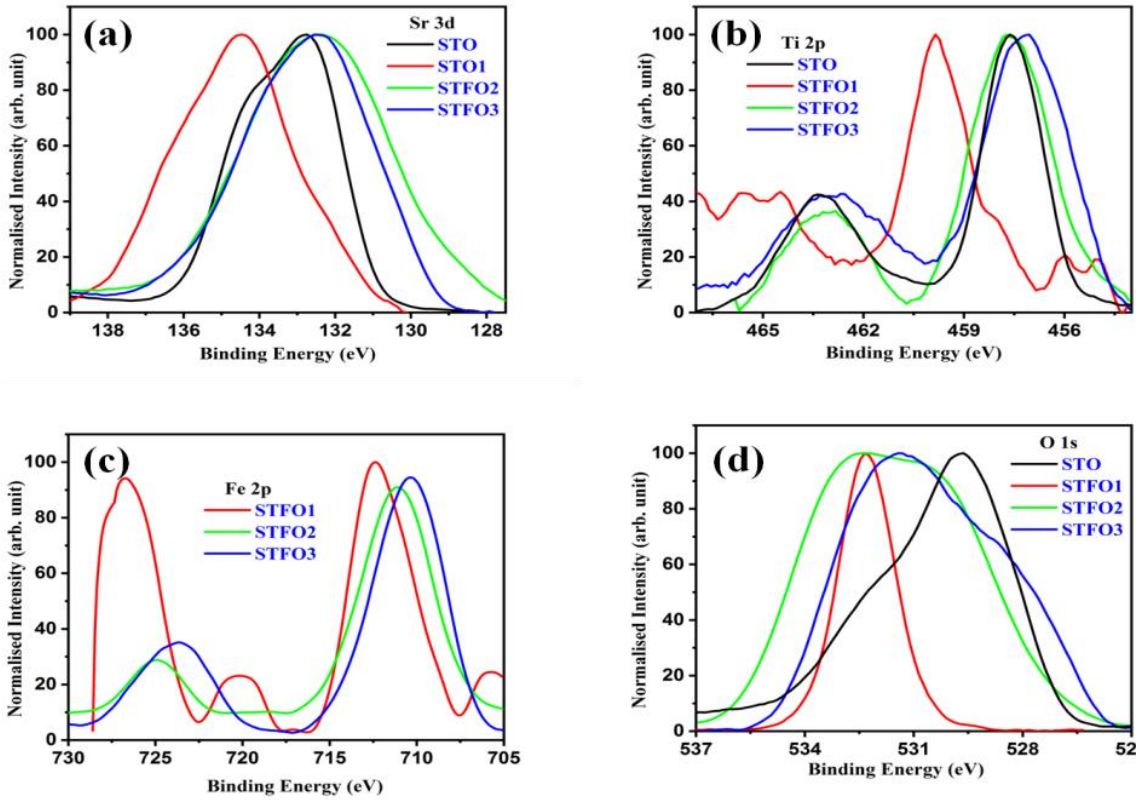

Fig. S6 Peak shifting of **(a)** Sr 3d, **(b)** Ti 2p, **(c)** Fe 2p, and **(d)** O 1s XPS spectra for elements in STO, STFO1, STFO2, and STFO3 samples.

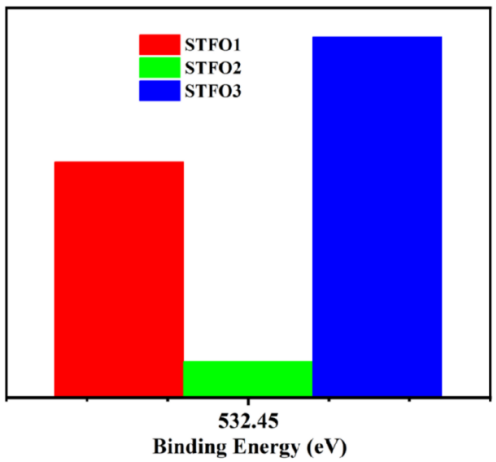

Fig. S7 Comparative areas of the highest O 1s XPS peaks with binding energies for STFO1, STFO2, and STFO3.

Table S5 Different Raman modes for Fe-doped STO in present work and published reports

Ref.	Raman shift for the mode appearing in spectrum/cm^{-1}			
	TO2	TO4	LO3	LO4
[S4]	171	540	–	800
[S9]	–	545	475	795
[S10]	178 [a)]	–	–	791
[S11]	170	539	–	793
This work	187	551	481	778

a) The first-order LO1/TO2 mode.

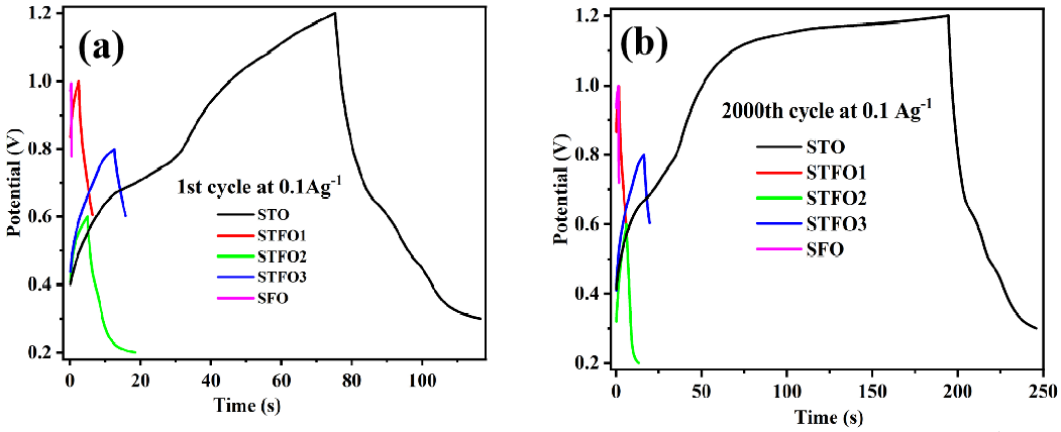

Fig. S8 GCD curves at **(a)** the 1st cycle and **(b)** the 2000th cycle at the current density of 0.1 $A \cdot g^{-1}$ for STO, SFO, and Fe-doped STO, revealing the response in potential with respect to time during charging and discharging process.

References

[S1] Wang X, Wang Z, Hub Q, et al. Room temperature multiferroic properties of Fe-doped nonstoichiometric $SrTiO_3$ ceramics at both A and B sites. Solid State Communications, 2019, 289: 22–26

[S2] Abdi M, Mahdikhani V, Sheibani S. Visible light photocatalytic performance of La-Fe co-doped $SrTiO_3$ perovskite powder. Optical Materials, 2020, 102: 109803

[S3] Li P, Liu C, Wu G, et al. Solvothermal synthesis and visible-light-driven photocatalytic degradation for tetracycline of Fe-doped $SrTiO_3$. RSC Advances, 2014, 88: 47129–47905

[S4] Fuentes S, Munoz P, Barraza N, et al. Structural characterisation of slightly Fe-doped $SrTiO_3$ grown via a sol–gel hydrothermal synthesis. Journal of Sol-Gel Science and Technology, 2015, 75: 593–601

[S5] Humayun M, Xu L, Zhou L, et al. Exceptional co-catalyst free photocatalytic activities of B and Fe co-doped $SrTiO_3$ for CO_2 conversion and H_2 evolution. Nano Research, 2018, 11(12): 6391-6404

[S6] Pramanik S, Mondal S, Mandal A C, et al. Role of oxygen vacancies on the green photoluminescence of microwave-assisted grown ZnO nanorods. Journal of Alloys and Compounds, 2020, 849: 156684

[S7] Kim D H, Aimon N M, Bi L, et al. The role of deposition conditions on the structure and magnetic properties of $SrTi_{1-x}Fe_xO_3$ films. Journal of Applied Physics, 2012, 111: 07A918

[S8] Li Y, Niu S, Hao Y, et al. Role of oxygen vacancy on activity of Fe-doped $SrTiO_3$ perovskite bifunctional catalysts for biodiesel production. Renewable Energy, 2022, 199: 1258–1271

[S9] Vracar M, Kuzmin A, Merkle R, et al. Jahn–Teller distortion around Fe^{4+} in $SrTi_{1-x}Fe_xO_3$ from X-ray absorption spectroscopy, X-ray diffraction, and vibrational spectroscopy. Physical Review B, 2007, 76: 174107

[S10] Pei Y, Zhang R, Song Y, et al. Emergent magnetic phase transitions in Fe-doped $SrTiO_{3-\delta}$. AIP Advances, 2019, 9: 125302

[S11] Minh N V, Phuong D T T. $SrTi_{1-x}Fe_xO_3$ nanoparticle: a study of structural, optical, impedance and magnetic properties. Journal of Experimental Nanoscience, 2011, 6(3): 226–237